Chemical Engineering Journal 225 (2013) 254–265

Contents lists available at SciVerse ScienceDirect

Chemical Engineering Journal

journal homepage: www.elsevier.com/locate/cej

One-pot electro-synthesis of ZrO_2–ZnO/HY nanocomposite for photocatalytic decolorization of various dye-contaminants

N. Sapawe [a], A.A. Jalil [a,*], S. Triwahyono [b]

[a] Institute of Hydrogen Economy, Faculty of Chemical Engineering, Universiti Teknologi Malaysia, 81310 UTM, Johor Bahru, Johor, Malaysia
[b] Ibnu Sina Institute for Fundamental Science Studies, Faculty of Science, Universiti Teknologi Malaysia, 81310 UTM, Johor Bahru, Johor, Malaysia

HIGHLIGHTS

- A new one-pot electrolysis method of Si with Zr and Zn catalyst was introduced.
- 1 wt% $EGZrO_2$–1 wt% EGZnO/HY exhibited superior performance for MB decolorization.
- High decolorization percentage (>80%) of MG, CR, and MO were achieved.

GRAPHICAL ABSTRACT

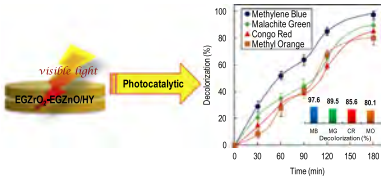

ARTICLE INFO

Article history:
Received 4 December 2012
Received in revised form 27 March 2013
Accepted 28 March 2013
Available online 11 April 2013

Keywords:
$EGZrO_2$–EGZnO/HY
Electrochemical
HY zeolite
Photodecolorization
Methylene blue
Dyes

ABSTRACT

A highly photoreactive electrogenerated catalyst ($EGZrO_2$–EGZnO/HY) was prepared by a facile one-pot electrochemical method. The restructuring of the aluminosilicate protonated Y zeolite (HY zeolite) framework presumably occurred during electrolysis via dealumination accompanied by the insertion of Zr and Zn ions resulting from anodic dissolution to form a new active species, Si coordinated with Zr and Zn in the HY framework. The photoactivity of the photocatalyst was examined by photodecolorization of methylene blue (MB) under varying pH, catalyst dosage, and initial concentrations of MB. An amount of 0.60 g L^{-1} 1 wt.% $EGZrO_2$–1 wt.% EGZnO/HY was found to be the optimum dosage for 10 mg L^{-1} MB, which gave almost complete photodecolorization of methylene blue after 1 h under visible light at pH 11 and room temperature. The photocatalytic reaction followed pseudo first-order kinetics which were rationalized in terms of the Langmuir–Hinshelwood model, and provided nearly complete mineralization. After five cycling runs, the catalyst was still stable and showed no leaching effect. High decolorization percentage (>80%) of other dyes such as malachite green (MG), Congo red (CR), and methyl orange (MO) were also obtained.

1. Introduction

There are several methods for the removal of organic pollutants, particularly dyes, that have been reported, including chemical and biological oxidation [1], adsorption [2], coagulation and flocculation [3], electrochemical [4], ion exchange [5], and membrane separation [6]. However, these methods have their own limitations as they are time-consuming, expensive, commercially unattractive, and generate secondary wastes [7].

Advanced oxidation processes (AOPs) using semiconductors such as TiO_2, ZnO, WO_3, Fe_2O_3, CuO, ZrO_2, and CdS as photocatalysts are an essential technique in wastewater treatment because they can convert a wide range of harmful dyes into non-toxic products, CO_2 and water at ambient temperatures [8–14]. The most popular metal oxide used is TiO_2, but ZnO has also attracted much attention due to its band gap energy, which is similar to TiO_2 (3.20 eV); it also demonstrates high photosensitivity and stability when degrading various pollutants [9,10]. In parallel, mixed metal oxides such as TiO_2–ZrO_2, Ag–ZnO, Fe_2O_3–TiO_2, Sn–ZnO and Ag–TiO_2 can also exhibit better performance and enhance the photocatalytic activity [9,11,15–17].

* Corresponding author. Tel.: +60 7 5535581; fax: +60 7 5536165.
E-mail address: aishah@cheme.utm.my (A.A. Jalil).

1385-8947/$ - see front matter © 2013 Elsevier B.V. All rights reserved.
http://dx.doi.org/10.1016/j.cej.2013.03.121

The use of mesoporous materials, such as zeolite, as a support for metal oxides (TiO_2–HZSM5, Co–ZSM5, CuO–X, CdS–zeolite A, and CdO–zeolite A) has become the focus of intensive research because these materials influence the catalytic performance through structural features [18–23]. Zeolitic materials offer high surface areas, are thermally stable, eco-friendly in nature, and have specific photophysical properties for controlling charge- and electron-transfer processes [24,25]. The interaction between zeolite and metal oxides also leads to an enhancement of the contact between the catalyst surface and irradiation, as well as a reduction in the amount of metal oxide required [26].

Recently, we reported a new preparation method for an α-Fe_2O_3 supported HY catalyst by a simple and rapid electrochemical process, which exhibited high photoactivity in the decolorization of methyl orange [8]. The nanosized metal oxides were found to play important roles in the enhancement of the reaction, as well as the synergistic effect provided by both metal oxide and support [27]. Accordingly, the EGZrO$_2$/HY and EGZnO/HY catalyst, which was prepared by the same method, also showed the best performance for the photodecolorization of methylene blue [28,29]. The introduction of a second metal improved and endowed extra properties to the photocatalyst by altering and restructuring the materials [11]; therefore, we attempted to prepare ZrO_2 and ZnO supported on HY zeolite by the corresponding method. ZrO_2 was chosen due to its specific optical and electrical properties, thermal stability, and strong mechanical strength as well as the presence of acid-base and redox capabilities [30–32].

For the first time, we report the facile synthesis of an electrogenerated ZrO_2 and ZnO supported HY (EGZrO$_2$–EGZnO/HY) catalyst and its remarkable performance regarding the photodecolorization of methylene blue (MB). The 1 wt.% EGZrO$_2$–1 wt.% EGZnO/HY photocatalyst was electrosynthesized in less than 4 min. The catalysts were then characterized by X-ray photoelectron spectroscopy (XPS), ^{29}Si and ^{27}Al magic angle spinning nuclear magnetic resonance (MAS NMR) imaging, Fourier transform infrared (FTIR) analysis, X-ray diffraction (XRD), transmission electron microscopy (TEM), field emission scanning electron microscopy (FE-SEM), Brunauer–Emmett–Teller surface area analysis (BET), ultraviolet–visible diffuse reflectance spectroscopy (UV–vis/DRS), and inductively coupled plasma mass spectrometry (ICP-MS). Based on the ^{29}Si and ^{27}Al MAS NMR, FTIR, and XPS results, a structure and reaction pathways for the formation of the new catalyst were also proposed. The performance of EGZrO$_2$–EGZnO/HY was compared with bare HY, EGZrO$_2$/HY, and EGZnO/HY catalysts and the appropriate conditions for photodecolorization were examined under varying pH levels, catalyst dosages and initial concentrations of MB. The kinetic behavior of the catalyst was also studied to determine the surface interaction of the catalyst with MB. The EGZrO$_2$–EGZnO/HY photocatalyst was then applied to other dyes such as malachite green (MG), Congo red (CR), and methyl orange (MO), in order to demonstrate the effectiveness of the photocatalyst used.

2. Experimental

2.1. Materials

The HY zeolite had a Si/Al ratio of 80 and was purchased from Zeolyst International. *N,N*-dimethylformamide (DMF) was purchased from Merck and naphthalene was obtained from Fluka. Sodium hydroxide, hydrochloric acid, methylene blue (C.I. 52015 for microscopy), malachite green, Congo red, and methyl orange were obtained from QReC^{TM}. The platinum (Pt), zirconia (Zr), and zinc (Zn) plate cells were obtained from Nilaco Metal, Japan. Degussa P25 TiO_2 was obtained from Acros Organics, Belgium. All of the reagents were analytical grade and were used as received. The deionized water was used for the preparation of pH solution. Adjustment of the pH solution was performed using a 0.1 M HCl and NaOH solution.

2.2. Catalyst preparation

1 wt.% EGZrO$_2$–1 wt.% EGZnO/HY catalyst was prepared according to the previous reported procedure [33,34]. A 10 mL DMF solution containing 0.1 M tetraethylammonium perchlorate was electrolyzed in the presence of 6 mmol naphthalene as a mediator and 1.5 g HY zeolite in a normal one-compartment cell fitted with a Pt plate cathode (2×2 cm^2) and a Zr plate anode (2×2 cm^2), then switched to a Zn plate anode (2×2 cm^2) at a constant current density of 120 mA/cm^2 under a nitrogen atmosphere at 273 K. After electrolysis the mixture was impregnated, oven dried overnight at 378 K, and calcined at 823 K for 3 h to yield a white powder, EGZrO$_2$–EGZnO/HY catalyst, which ready for characterization and photocatalytic testing.

The bare EGZrO$_2$ and EGZnO were prepared using the same procedure as above but in the absence of HY zeolite. The required weight percent of the EGZrO$_2$ and EGZnO supported on HY was calculated by the time of electrolysis, which is based on the Faraday's law,

$$t = \left(\frac{F}{I}\right)(z \times n) \quad (1)$$

where t is the total time for the constant current applied (s); F is the 96,486 C mol^{-1}, which is the Faraday constant; I is the electric current applied (mA); z is the valency number of ions of substance (electrons transferred per ion); and n is the number of moles of substance (number of moles, liberated n = m/M).

2.3. Characterization

The chemical oxidation state of the EGZrO$_2$–EGZnO/HY catalyst was determined using XPS conducted on a Kratos Ultra spectrometer equipped with a Mg Kα radiation source (10 mA, 15 kV) in the range of 0–800 eV. The powdered sample was pressed into a small Inox cylinder and analyzed inside an analysis chamber at 1×10^{-10} Pa during data acquisition. To correct the energy shift due to surface charging of the samples, the binding energy of the C_{1s} peak at 284.5 ± 0.1 eV was taken as the internal standard. ^{29}Si and ^{27}Al MAS NMR spectra were recorded on a Bruker Solid NMR (JEOL 400 MHz) spectrometer using tetramethylsilane (TMS) as an external reference at room temperature.

FTIR (Perkin Elmer Spectrum GX FTIR Spectrometer) was performed using the KBr method with a scan range of 400–4000 cm^{-1}. The crystalline structures of the catalysts were studied by XRD recorded on a D8 ADVANCE Bruker X-ray diffractometer using Cu Kα radiation at a 2θ angle ranging from 3° to 90°. The particle sizes of the catalysts were calculated using the Debye–Scherrer equation,

$$D = \frac{k\lambda}{\beta \cos \theta} \quad (2)$$

where k = 0.94 is a coefficient, λ = 1.5406 Å is the X-ray wavelength, β is the full width half maximum (FWHM) of the sample and θ is the diffracting angle. The phases were identified with the aid of the Joint Committee on Powder Diffraction Standards (JCPDS) files.

The morphological properties of the EGZrO$_2$–EGZnO/HY catalyst as well as the distribution of EGZrO$_2$–EGZnO deposited on the HY surface were examined by TEM (JEOL JEM-2100F). The topological properties of the catalysts were observed by FE-SEM (JSM-6701F). The textural properties (i.e., specific surface area, pore volume, and pore diameter) were determined from

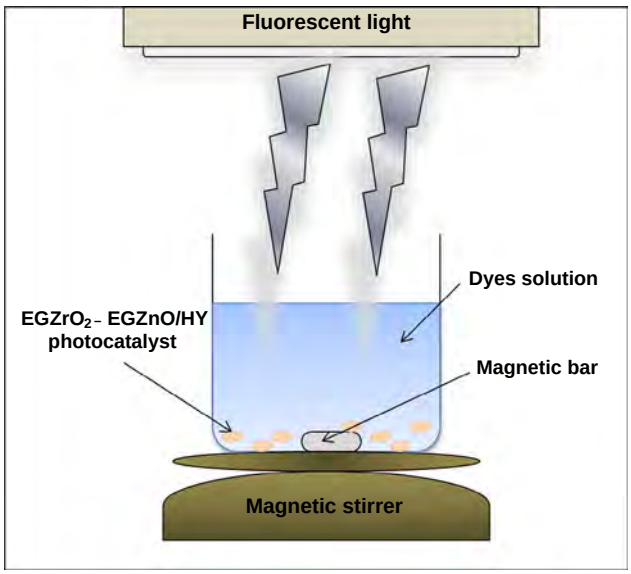

Fig. 1. Schematic diagram of the photocatalytic reaction.

nitrogen adsorption–desorption isotherms at liquid nitrogen temperature using a Micromeritics ASAP 2010 instrument. The surface area was calculated with the BET method, and pore distributions were determined by the Barrett–Joyner–Halender (BJH) method. Prior to measurement, all the samples were degassed at 383 K to 0.1 Pa. The optical absorption properties of the catalyst were obtained using a UV–vis DRS (Perkin Elmer Spectrophotometer) in the range of 200–800 nm at room temperature. The band gap of $EGZrO_2$, EGZnO, and $EGZrO_2$–EGZnO was determined from plots of the Kubelka–Munk (K–M) function $[f_{K-M} = (h\nu/\lambda)^{1/2}]$ as a function of the energy of the excitation light $[h\nu]$.

2.4. Photocatalytic testing

The photocatalytic activity of the prepared $EGZrO_2$–EGZnO/HY catalyst was tested for the decolorization of MB using a batch experimental set up as shown in Fig. 1. A 0.12 g of the catalyst in powder form was dispersed in 200 mL of 10 mg L^{-1} MB aqueous solution. The adsorption–desorption equilibrium was achieved under dark conditions after 1 h, and the mixture was then irradiated at room temperature for 1.5 h with constant stirring using a fluorescent lamp (Philips TLD 36 W/865; 15,000 h; 6500 K; 420–520 nm emission). At specific time intervals, 2.5 mL of the sample solution was withdrawn and centrifuged prior measurements for the remaining MB concentration by a UV–vis spectrophotometer (Thermo Scientific Genesys 10 uv Scanning) using the characteristic adsorption band at 664 nm. In addition, the characteristic adsorption band of MG, CR, and MO dye were observed at 616 nm, 498 nm, and 464 nm, in respectively. The decolorization percentage was calculated as follows,

$$\text{Decolorization } (\%) = \frac{(C_0 - C_t)}{C_0} \times 100 \quad (3)$$

where C_0 represents the initial concentration and C_t denotes a variable concentration.

2.5. Analyses

The elemental analyses of Zr and Zn in a solution during an experiment were determined by ICP-MS using ELAN 6100 Perkin Elmer ICPMS. The HACH DR4000 spectrometer was used for chemical oxygen demand (COD) measurement. In addition, the total organic carbon (TOC) removal was determined using a TOC Shimadzu Vcph spectrophotometer for each run before and after a 1.5 h reaction time for the evaluation of the mineralization of MB dye. TOC was calculated as the difference between the total carbon (TC) and inorganic (IC) in the liquid sample.

3. Results and discussion

3.1. Characterization

3.1.1. Chemical oxidation state determination

XPS analyses were performed to determine the chemical states of Zr and Zn in the catalyst (Fig. 2a and b). A doublet peak with binding energies of 183.1 eV ($Zr_{3d5/2}$) and 185.2 eV ($Zr_{3d3/2}$) was observed, which exactly matched the chemical oxidation state of Zr^{4+} ions [35]. The $Zn_{2p3/2}$ peak at 1022.4 eV corresponds to the characteristic peak of Zn^{2+} [36]. However, the observed value for the $EGZrO_2$–EGZnO/HY sample was slightly shifted to higher binding energies, compared to the reported values of pure ZrO_2 (182.2 eV and 184.5 eV) and ZnO (1021.2 eV), suggesting an interaction between the $EGZrO_2$–EGZnO and HY [31,37]. Atom of a higher positive oxidation state exhibit a higher binding energy due to the extra coulombic interaction between the photo-emitted electron and the ion core, therefore, discriminate between different oxidation states and chemical environments. In this case, Si is more electronegative and was expected to withdraw more electron density that implies a shift of the binding energies to higher values [28,38,39].

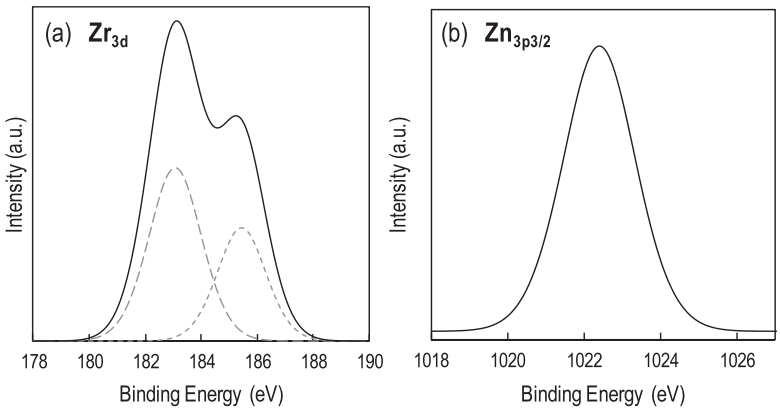

Fig. 2. XPS spectra of (a) Zr_{3d} and (b) $Zn_{2p3/2}$ for $EGZrO_2$–EGZnO/HY catalyst.

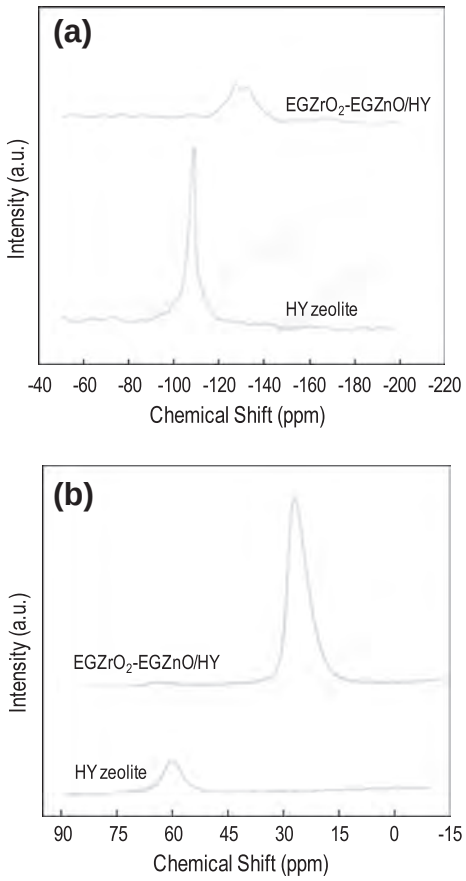

Fig. 3. MAS NMR spectra of (a) ^{29}Si, and (b) ^{27}Al of bare HY and $EGZrO_2$–EGZnO/HY catalyst.

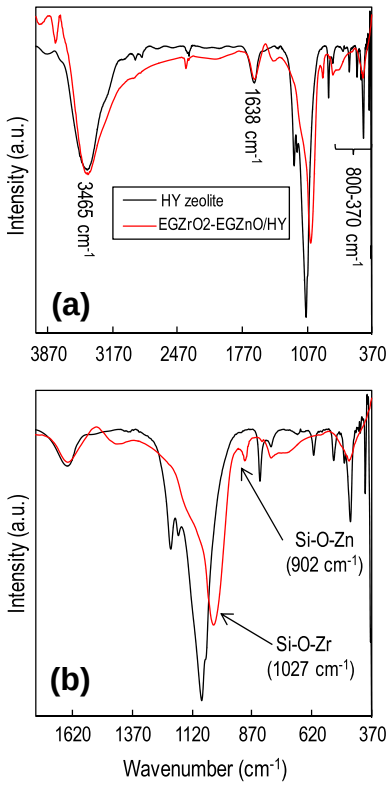

Fig. 4. FTIR spectra of catalysts at region (a) 4000–370 and (b) 1770–370 cm^{-1}.

3.1.2. Nuclear magnetic resonance

^{29}Si MAS NMR chemical shifts were used to define the Si environments and provide information regarding the coordination of Si. As illustrated in Fig. 3a, the intensity of the sharp peak observed for bare HY at −107 ppm was shifted to a higher ppm for $EGZrO_2$–EGZnO/HY. A doublet peak at −120 to −140 ppm is characteristic of a six-coordinated Si environment, as reported in the literature [40–42]. Next, ^{27}Al MAS NMR was employed to distinguish Al in framework sites or extra-framework sites (non-framework). Fig. 3b indicates that the peak corresponding to the tetrahedral Al framework in HY was eliminated when $EGZrO_2$–EGZnO was added and a new peak appeared at 29 ppm. According to Klinowski, this peak corresponds to the presence of penta-coordinated aluminum (non-framework) [43].

To clarify the substitution of Zr or Zn into the HY framework, the amount of unbounded Zr and Zn in the framework was studied. The corresponding catalyst was stirred in a DMF solution for 30 min and then filtered before being subjected to ICP-MS analysis. It was found that 1.58×10^{18} Zr and 1.20×10^{19} Zn atoms were

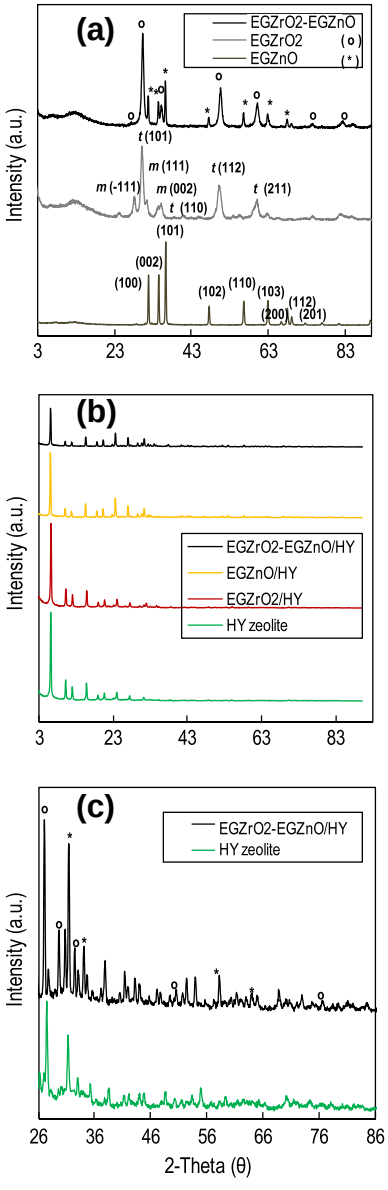

Fig. 5. XRD patterns of catalysts (a) and (b) for full range 3–83° and (c) for range 26–86°.

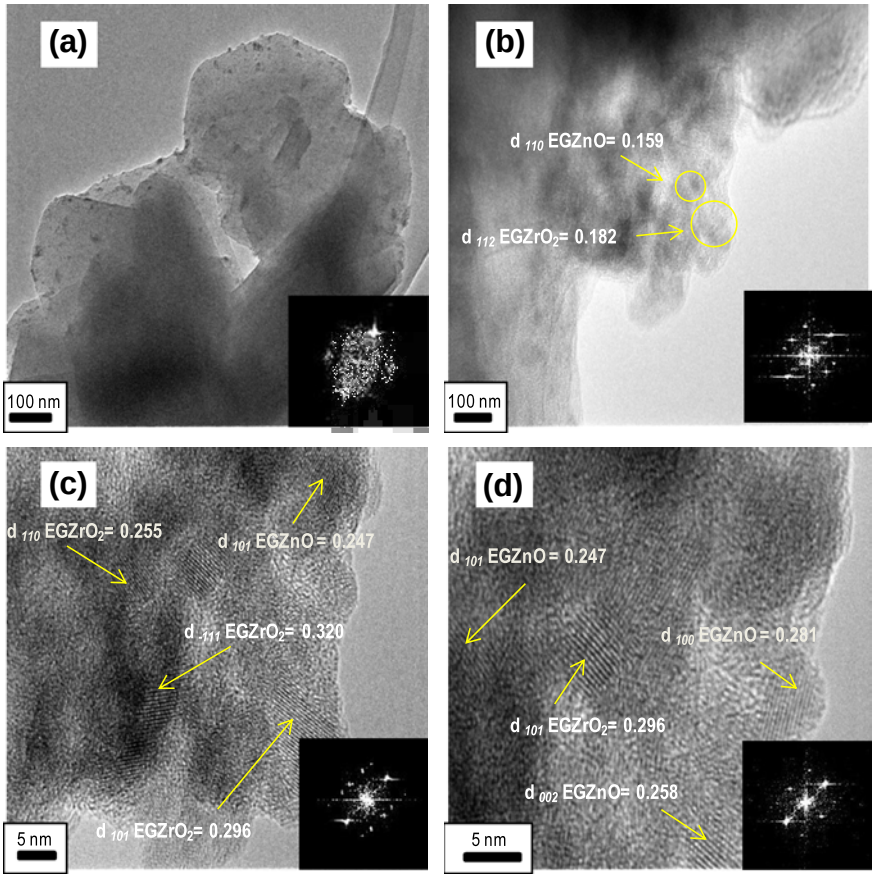

Fig. 6. TEM micrographs of (a–d) $EGZrO_2$–EGZnO/HY in low and high magnification and the insert of Fig. 5 (a–d) are its corresponding FFT.

detected in the filtrate solution, referring to unbound $EGZrO_2$ (1.6%) and EGZnO (8.7%). Therefore, 98.4% of Zr and 91.3% of Zn ions appeared to be bound to the HY framework. All of the calculations were based on the ratio of elements in HY, $(Al_7Si_{17}O_{48})\cdot 32(H_2O)$.

3.1.3. Vibrational spectroscopy

Fig. 4a shows the FTIR spectra of the prepared catalysts, which demonstrate a broad band at 3465 cm^{-1} due to the H_2O molecules adsorbed on the catalyst surface, and at 1638 cm^{-1}, attributed to the vibrational distortion of O–H groups on the catalyst surface. The peak at 1220 cm^{-1} was attributed to the δ_{OH} vibration of the hydrogen bonded OH groups of the HY and disappeared after the addition of $EGZrO_2$–EGZnO, this may be due to overlapping with the broad band at 1027 cm^{-1}. The γ_{OH} vibration at 820 cm^{-1} reduces after metal oxides loading due to the interaction of the molecules [44]. The weak bands between 800 and 370 cm^{-1}, which correspond to the Si–O–Si flexural vibration, decreased in intensity with $EGZrO_2$–EGZnO loading, signifying the possible superposition of Si–O–Si and Si–O–M bonds (M = Zr, Zn) [45]. An obvious band was observed at 1027 cm^{-1}, corresponding to the vibration of the Si–O–Zr bonds, verifying that Zr was inserted into the zeolite framework (Fig. 4b) [46]. The formation of Si–O–Zn bonds was confirmed by the existence of the corresponding peak at 902 cm^{-1} (Fig. 4b) [47].

3.1.4. Crystallinity, phase and structural studies

The XRD pattern of the prepared $EGZrO_2$–EGZnO/HY catalysts was compared with $EGZrO_2$, EGZnO, $EGZrO_2$–EGZnO, and bare HY, and the results are shown in Fig. 5. Almost all of the peaks corresponding to $EGZrO_2$ and EGZnO were detected in $EGZrO_2$–EGZnO, indicating that the prepared catalysts were well-mixed (Fig. 5a). A series of peaks were observed for $EGZrO_2$ and EGZnO, which is consistent with the tetragonal and monoclinic phase of ZrO_2 (JCPDS file PDF No. 01-072-2743), and the hexagonal wurtzite structure of ZnO (JCPDS file PDF No. 01-071-6424), respectively, with no other diffraction peaks being detected. This indicates the purity of the prepared catalysts [10,48,49].

Table 1
The *d*-value of $EGZrO_2$ and EGZnO lattice obtained from XRD and TEM analysis.

2-Theta (θ)[a]	*hkl*	d_{hkl}[a] (Å)	*d*-spacing[b] (nm)
$EGZrO_2$			
28.2	−111	3.16	0.320
30.2	101	2.95	0.296
31.5	111	2.83	nd
34.5	002	2.59	nd
35.2	110	2.54	0.255
50.3	112	1.81	0.182
60.2	211	1.54	nd
EGZnO			
31.9	100	2.80	0.281
34.6	002	2.59	0.258
36.4	101	2.47	0.247
47.7	102	1.91	nd
56.7	110	1.62	0.159
63.0	103	1.47	nd
66.5	200	1.40	nd
68.1	112	1.38	nd
69.2	201	1.36	nd

[nd] Not detected
[a] Value obtained from XRD analysis.
[b] Lattice fringes obtained from TEM analysis.

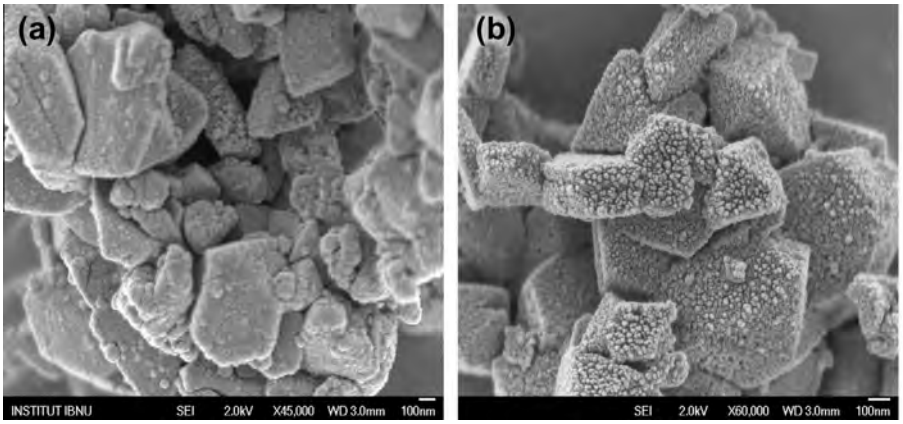

Fig. 7. FE-SEM images of $EGZrO_2$–EGZnO/HY catalyst in (a) 45,000× and (b) 60,000× magnification.

The peak intensity of HY decreased as $EGZrO_2$ and EGZnO were loaded onto HY (Fig. 5b). This suggested that the presence of foreign substances affected the morphology of the supported HY fingerprint. Fig. 5c shows the enlargement of a selected area of an XRD pattern from 26° to 86° for $EGZrO_2$–EGZnO/HY and bare HY. There are several peaks detected which correspond to ZrO_2 and ZnO, verifying the presence of $EGZrO_2$ and EGZnO metals in the HY framework.

The average crystallite size of the metal oxide catalysts was estimated using the Debye–Scherrer equation on the basis of the major peaks of $EGZrO_2$ (101) and EGZnO (101), which are 14.6 nm and 30.2 nm, respectively. However, the crystallite size of both metal oxides in the hybrid $EGZrO_2$–EGZnO catalyst increased to 15.4 nm and 33.2 nm, respectively, which may be due to interaction between the zirconia and zinc species [50].

3.1.5. Morphological properties

The morphological properties of the $EGZrO_2$–EGZnO/HY catalysts were examined by HR-TEM, and the images are shown in Fig. 6a–d. The inset images show the Fast Fourier Transform patterns (FFT), and the magnification of the selected areas in the FFT patterns shows the atomic arrangement of the crystal, which allowed the estimation of the inter-planar distance. The value of the inter-planar distance (*d*-spacing) of the lattice fringes estimated from this image was consistent with the value of the lattice spacing of $EGZrO_2$ and EGZnO obtained from the XRD analysis, which is tabulated in Table 1. Based on this result, it was confirmed that $EGZrO_2$ and EGZnO existed in the HY support, which is in agreement with the FTIR result.

3.1.6. Topological properties

The topological properties of the EGZnO and EGZnO/HY catalysts were studied by FE-SEM and the results are shown in Fig. 7. The influence of the addition of zirconia and zinc on the HY zeolite structure can also be confirmed from SEM images. The micrographs show the presence of small crystallites like uniformly distributed along some intergrowth. The fine particles of zirconia and zinc oxide may be well dispersed but their presence did not result in significant contrast at magnification up to 60,000×. Smooth surface with multi-dimensional of 1 wt.% $EGZrO_2$–1 wt.% EGZnO/HY catalyst was observed that could provide better contact angle area to light penetration, thereby improving the utilization rate of photodecolorization of MB [16].

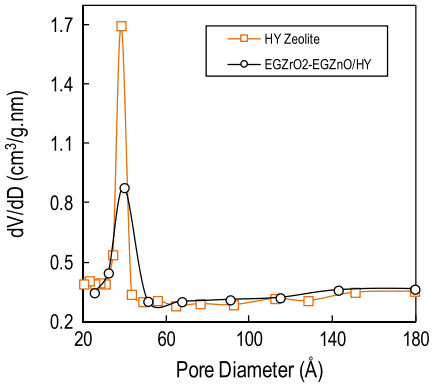

Fig. 8. Pore size distribution curves of catalysts.

3.1.7. Study of textural properties

The surface area analysis data obtained from the BET method and the pore volume and pore diameter determined by the Barrett–Joyner–Halenda (BJH) desorption isotherms method are presented in Table 2. The addition of $EGZrO_2$–EGZnO onto HY decreased the surface area and pore volume of the catalysts resulting in blockage of the pores (Fig. 8), and increased the pore diameter, which may be attributed to the uneven particle sizes of the metal oxides. The improvement in the surface contact of the catalyst after the modification of both metal oxides and HY enhanced light irradiation, thereby increasing the photodecolorization of MB. A similar observation was also reported for the photoreduction of methyl orange by TiO_2 supported on a zeolite matrix [51].

Table 2
The textural properties of the catalysts.

Catalysts	Surface area ($m^2\ g^{-1}$)	Average pore diameter[a] (nm)	Pore volume ($cm^3\ g^{-1}$)
$EGZrO_2$	54.9	11.1	0.153
EGZnO	61.3	6.37	0.263
$EGZrO_2$–EGZnO	138	5.69	0.325
HY	654	2.73	0.447
$EGZrO_2$–EGZnO/HY	536	2.76	0.439

[a] Adsorption average pore diameter (4 V/V by BET).

3.1.8. Study of optical properties

Fig. 9a shows the UV–Vis reflectance spectra of the prepared catalysts. Both $EGZrO_2$ and EGZnO resulted in a blue shift at 245 nm and 386 nm, respectively, signifying that the photoreaction was suitable to be conducted in the UV light region. However, the combination of $EGZrO_2$ and EGZnO improved and enhanced

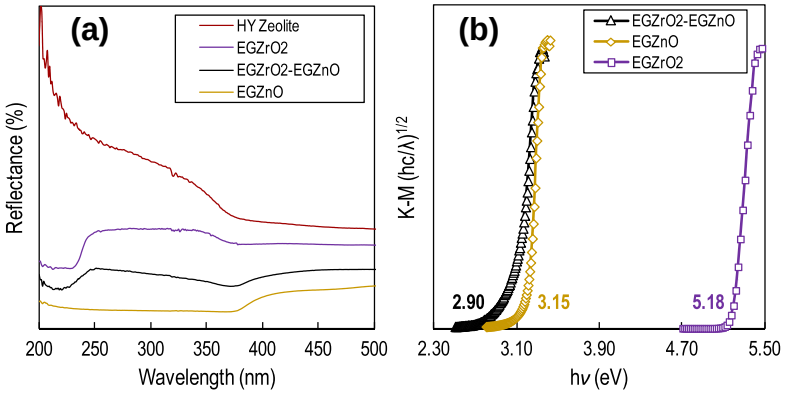

Fig. 9. (a) UV–vis reflectance spectra of catalysts and (b) the (f_{K-M}) vs. ($h\nu$) spectra of catalysts.

their optical properties (the band gap energy was reduced to 2.90 eV) [52,53]. The outcome of this sort of modification suggests that the $EGZrO_2$–EGZnO/HY catalyst was preferable and capable of performing under visible light conditions. The band gap energies of $EGZrO_2$, EGZnO, and $EGZrO_2$–EGZnO were determined using the Kubelka–Munk (K–M) spectrum by plotting $f_{K-M} = (hc/\lambda)^2$ as a function of $h\nu$; the results are shown in Fig. 9b [54]. The band gap values of $EGZrO_2$ and EGZnO were similar and agree with those reported in the literature [55].

3.1.9. Reaction pathways of the $EGZrO_2$–EGZnO/HY photocatalyst

Probable reaction pathways of the constitution of $EGZrO_2$–EGZnO/HY are shown in Fig. 10, on the basis of restructuring the aluminosilicate HY framework. During electrolysis, dealumination of HY occurred and formed non-framework Al, $(AlO_5)^+$, which provided an oxygen source in combination with the oxygen from the framework and allowed the insertion of the Zr ions, resulting from the anodic dissolution, to form Si–O–Zr [8,28,33,56]. Afterwards, a similar phenomenon also occurred for Zn ions when the Zr anode was switched to a Zn anode, which finally gave the $EGZrO_2$–EGZnO/HY catalyst. The presence of a nucleophilic agent (DMF) in the reaction may also have been responsible for the formation of the transition state of Si into the six-coordinated state of Si [57]. On the other hand, electron transfer from naphthalene radical anions at the cathode also occurred to form pure metals ($EGZr^0$ and $EGZn^0$), which then were oxidized to $EGZrO_2$ and EGZnO during calcination [34].

The formation of penta-coordinated Al was detected by ^{27}Al MAS NMR. The FTIR results obtained confirmed the presence of Si–O–Zr and Si–O–Zn bonds in the catalyst. The XPS spectra of Zr_{3d} and $Zn_{2p3/2}$ established the chemical oxidation state of Zr^{4+} and Zn^{2+} ions, respectively. Therefore, it was proposed that dealumination occurred and then Zr and Zn filled in the Si sites in the HY framework during electrolysis. In addition, the ^{29}Si MAS NMR spectra demonstrated six-coordinated Si, and the total number of unbound Zr and Zn atoms in the framework obtained by ICP-MS also supports this result. This study also showed that dealumination followed by restructuring of the aluminosilicate HY framework could be performed easily by the electrolysis system without using strong acids, reactive compounds, and/or hydrothermal treatment [58]. However, the exact structure of $EGZrO_2$–EGZnO/HY is still under study.

3.2. Photocatalytic testing for the decolorization of MB

3.2.1. Catalyst performance

The photoactivity of the prepared $EGZrO_2$–EGZnO/HY catalyst was tested and compared with $EGZrO_2$/HY, EGZnO/HY, Degussa P25 TiO_2, and bare HY on the decolorization of MB (Fig. 11). Each experiment was performed in the dark for 1 h to achieve

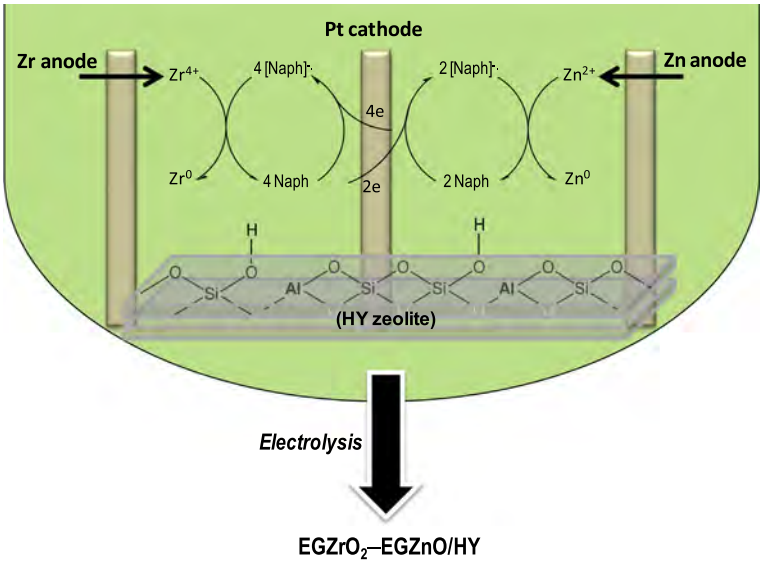

Fig. 10. Proposed mechanism for the formation of a Si coordinated with Zr and Zn catalyst.

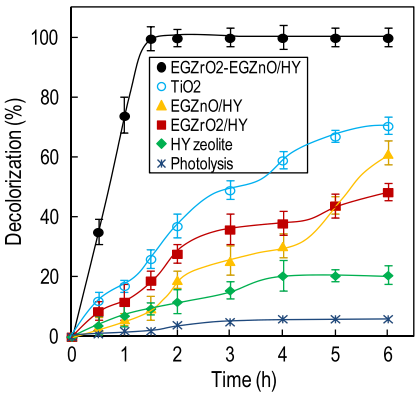

Fig. 11. Catalyts performance on decolorization of MB [C_{MB} = 10 mg L^{-1}, pH = 11, W = 0.60 g L^{-1}, t = 6 h, 303 K].

adsorption–desorption equilibrium before irradiation under a fluorescent lamp at room temperature for 6 h with constant stirring. The results show that complete decolorization of MB was achieved within a very short contact time (1.5 h) under visible light conditions when using $EGZrO_2$–EGZnO/HY, indicating the high photoactivity of Si coordinated with the Zr and Zn catalyst compared to the other catalysts. $EGZrO_2$/HY, EGZnO/HY, and TiO_2 demonstrated lower activity, with <80% of MB decolorization under the studied conditions after 6 h of contact time. In addition, a control experiment was also conducted under photolysis conditions which gave only 6% MB decolorization following a long period of exposure to fluorescent light (6 h) with constant stirring (Fig. 11).

3.2.2. Effect of pH

The effect of pH on MB decolorization using the $EGZrO_2$–EGZnO/HY catalyst was studied in the pH range of 3–11 under visible light conditions; the results are presented in Fig. 12a. The highest level of decolorization was obtained at pH 11 with total decolorization of 99.7%, whereas the other results were 75.2%, 63.9%, 65.7%, and 76.9%, at pH 9, pH 7, pH 5, and pH 3, respectively. The amphoteric behavior influences the surface charge properties of the catalyst when the photoreaction occurs on the surface of semiconductor [59]. This behavior can be described on the basis of zero point charge (pH_{zpc}) of the $EGZrO_2$–EGZnO/HY, which was determined to be at pH 6.4 (Fig. 12b). At pH > 6.4, the surface of the $EGZrO_2$–EGZnO/HY became negatively charged, thus the MB cations are easily attracted to the catalyst surface. Besides, the exposure of abundance hydroxyl anions to visible light at pH 11 increased the formation of hydroxyl radicals and the photocatalytic reaction rate, which led to an increase in MB decolorization up to 99.7% after 1.5 h of contact time. Similar results were reported in the literature regarding the photodecolorization of MB using a CuO/X zeolite at pH 11 [20].

However, lowering the pH to acidic conditions caused the surface of the $EGZrO_2$–EGZnO/HY became positively charged and this inhibited the dye cations from approaching the catalyst surface, thus reduced the efficiency of the reaction to 76.9%. The same phenomenon was reported in the decolorization of methylene blue in the presence of TiO_2/ZnS nanocomposites under acidic conditions [60]. In contrast, changing the conditions to a neutral pH appeared to decrease the photocatalytic activity. This may be due to the surface of the catalyst was in zero net charged (pH_{zpc} = 6.4). In addition, the hydroxyl formation reduced under neutral conditions, resulting in fewer radicals being generated via an electron–hole pair, which is the most crucial factor for the initiation of photodecolorization activity. Therefore, the reaction did not perform well under neutral conditions. The nanosized ZnO was also found to be stable at alkaline pH (>pH 10) in term of dissolution and good photoactivity as well [61]. In this study, the introduction of second metal, $EGZrO_2$ toward EGZnO is believed to make this catalyst more stable. Generally, the passivity region (Pourbaix diagram) of ZnO begins at pH around 8.2–12.1, and note that the thermodynamic calculation predictions may contradict to the experimental result [62].

3.2.3. Effect of catalyst dosage

Fig. 13 shows the effect of catalyst dosages ranging from 0.10 to 1.20 g L^{-1} on MB decolorization. The increase in decolorization percentage was most likely the result of an increase in the number of active sites with higher amounts of catalyst loading, which contributed to an increase in the number of photons and dye molecules absorbed [50]. The most effective decolorization of MB was achieved with a catalyst dosage of 0.60 g L^{-1}, while a further increase in the catalyst dosage resulted in a decrease in decolorization. Higher particle concentrations led to greater turbidity of the suspension, which reduced light penetration and inhibited photodecolorization [63].

3.3. Kinetic analysis

To study the kinetics of MB photodecolorization, a series of reactions were performed at pH 11 with different initial concentrations of MB ranging from 10 to 100 mg L^{-1} (Table 3). The results of the experiment demonstrated that the concentration of 10 mg L^{-1} gave almost complete decolorization (99.7%) after 1.5 h of irradiation. Higher concentrations showed lower efficiency of

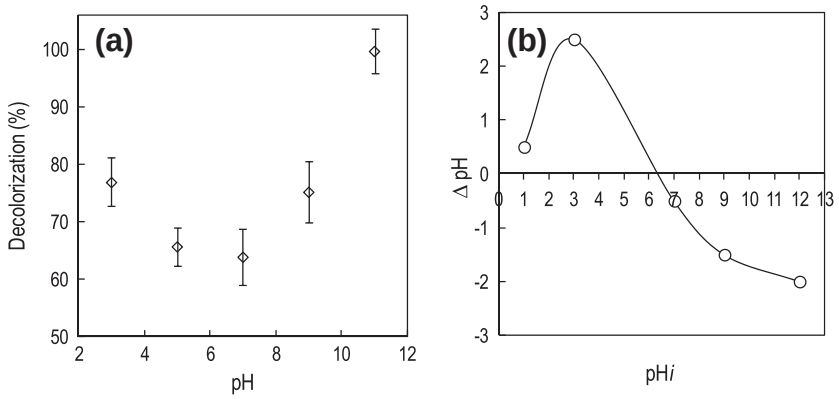

Fig. 12. Effect of pH on decolorization of MB [C_0 = 10 mg L^{-1}, W = 0.60 g L^{-1}, t = 1.5 h, $EGZrO_2$–EGZnO/HY, 303 K] and (b) the isoelectric point (pH_{zpc}) of the $EGZrO_2$–EGZnO/HY catalyst.

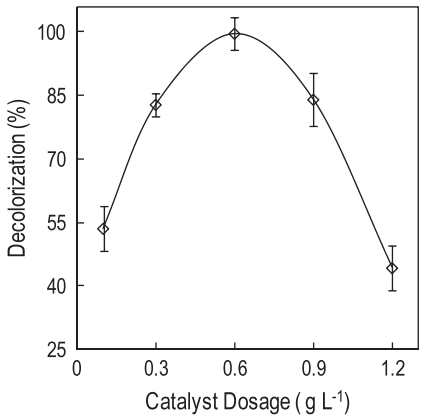

Fig. 13. Effect of catalyst dosage on decolorization of MB [C_0 = 10 mg L^{-1}, pH = 11, t = 1.5 h, $EGZrO_2$–EGZnO/HY, 303 K].

Table 3
The kinetics parameters of photodecolorization at different initial concentration of MB.

Initial concentration (mg L^{-1})	Reaction rate, k (h^{-1})	Initial reaction rate, r_o (mg L^{-1} h^{-1})	Decolorization (%)
10	1.21	12.1	99.7
20	0.840	16.8	78.7
30	0.453	13.6	50.6
50	0.290	14.5	33.1
70	0.204	14.2	21.2
100	0.143	14.3	15.6

photocatalytic decolorization due to the formation of several layers of adsorbed dye on the catalyst surface, which was increased at higher dye concentrations. In addition, large amounts of adsorbed dye were found to inhibit the reaction with the dye molecules, since there was no direct contact of the catalyst with photogenerated holes or hydroxyl radicals [64]. An increase in the dye concentration also prevented the dye molecules from reaching the catalyst surface in order to adsorb light and photons.

Generally, the influence of the initial concentration of most organic compounds on the photocatalytic decolorization rate is described by pseudo first-order kinetics, which is rationalized in terms of the Langmuir–Hinshelwood model that can be modified to accommodate reactions occurring at a solid–liquid interface [65]. At low initial dye concentrations, the simplest equation for the rate of photodecolorization of MB is given by:

$$\ln\ C_t = -kt + \ln\ C_0 \tag{4}$$

where k is the pseudo first-order rate, and C_0 and C_t are the concentrations of MB at the start and at time t, respectively. The integration of Eq. (4) yields Eq. (5):

$$\ln\ \left(\frac{C_0}{C_t}\right) = kt \tag{5}$$

The straight line resulting from a plot of ln (C_0/C_t) as a function of time shown in Fig. 14a confirmed that MB photodecolorization catalyzed by $EGZrO_2$–EGZnO/HY follows a pseudo first-order kinetics model. The slope of the line is the apparent first-order rate constant (k_{app}). The values of k obtained from these experiments are listed in Table 3 and reveal a significant and favorable effect of $EGZrO_2$–EGZnO/HY on the photodecolorization of MB. A lower concentration of MB resulted in a higher first-order rate constant, demonstrating the suitability of the system for low dye concentrations. Indeed, the concentration of dye in wastewater from textile industry effluents is always in the range of 10–50 mg L^{-1} [66].

Hypothetically, the photodecolorization of MB by $EGZrO_2$–EGZnO/HY could be an interface process [67], which might follow the Langmuir–Hinshelwood model (Eqs. (6) and (7)):

$$r_0 = -\frac{dC}{dt} = \frac{K_R K_{LH} C_0}{1 + K_{LH} C_0} = k_{app} C_0 \tag{6}$$

$$\frac{1}{k_{app}} = \frac{1}{K_R K_{LH}} + \frac{C_0}{K_R} \tag{7}$$

where K_R is the reaction rate constant and K_{LH} is the Langmuir–Hinshelwood adsorption equilibrium constant.

A linear plot was obtained by plotting $1/k_{app}$ as a function of C_0 (Fig. 14b), indicating that the photodecolorization of MB by $EGZrO_2$–EGZnO/HY is consistent with the Langmuir–Hinshelwood model. The reaction rate constant and the adsorption equilibrium constant were calculated to be K_R = 14.3 mg L^{-1} h^{-1} and K_{LH} = 7.49 L mg^{-1}, respectively. Since the value of K_R was larger than K_{LH}, these results suggest that the dye adsorption was the controlling step of the process [68,69].

3.4. Leaching and reusability of photocatalyst

To study the effect of zirconia–zinc leaching into the solution, the samples were kept in the dark for 1 h and then irradiated under fluorescent light for 1.5 h using an amount of 0.60 g L^{-1} 1 wt.% $EGZrO_2$–1 wt.% EGZnO/HY for 10 mg L^{-1} MB, at pH 11 and at room temperature before being subjected to ICP-MS. The results showed that no Zr and/or Zn ions were detected, indicating that the

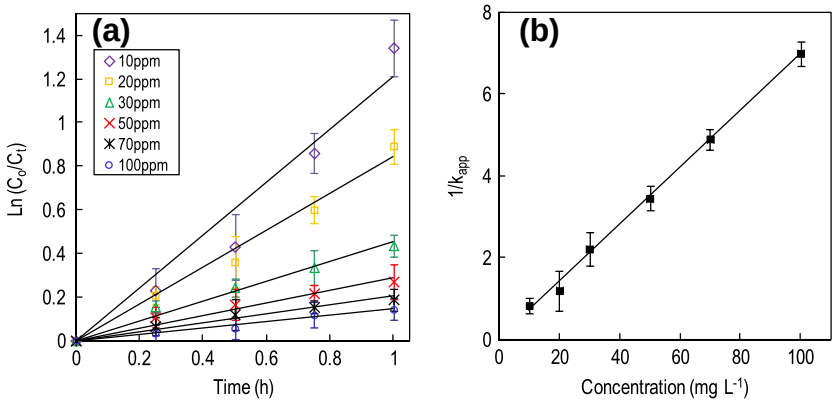

Fig. 14. (a) Photodecolorization kinetics of MB using $EGZrO_2$–EGZnO/HY at different MB concentrations and (b) the relationship between $1/k_{app}$ and initial concentration of MB.

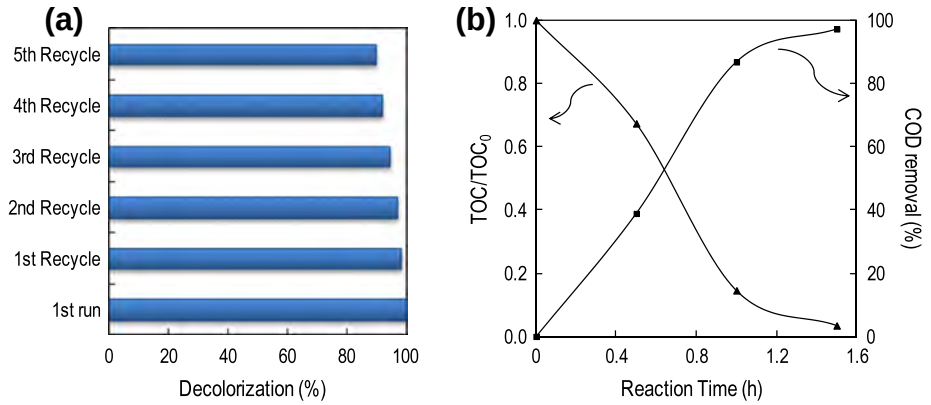

Fig. 15. (a) Reusability of $EGZrO_2$–EGZnO/HY on photocatalytic decolorization of MB [C_0 = 10 mg L^{-1}, pH = 11, W = 0.60 g L^{-1}, t = 1.5 h, 303 K] and (b) the COD removal and TOC reduction levels [C_0 = 10 mg L^{-1}, pH = 11, W = 0.60 g L^{-1}, t = 1.5 h, $EGZrO_2$–EGZnO/HY, 303 K].

occurrence of photocatalysis is mainly due to the Zr and/or Zn that exists on the catalyst surface.

Cycling runs for MB decolorization were also performed to evaluate the photocatalytic activity of $EGZrO_2$–EGZnO/HY (Fig. 15a). The initial concentration of MB was maintained (10 mg L^{-1}) at pH 11 for 1.5 h of irradiation time, and the catalyst was recycled after filtration and calcination at 823 K for 3 h after every cycle. A high degree of MB decolorization (>90%) was maintained after 9 h with five cycles run without any obvious catalyst deactivation [8,28,29].

3.5. Investigation on biodegradability

The chemical oxygen demand (COD) and total organic carbon (TOC) for the MB solution were measured; the results are shown in Fig. 15b. Indirectly, the COD was used to investigate the amount of organic compounds that were present in the aqueous solution. The initial COD value of the dye solution was found to be 144 mg L^{-1}, and was reduced to 4 mg L^{-1} after irradiation with fluorescent light for 1.5 h. The graph shows that the percentage of COD increased rapidly during the first 1 h of reaction, which may be due to the degradation of MB into two different compounds of hydroxylated and amine-substituent products, and then gradually increased until the reaction was completed. The hydroxylated compound was converted into a sulfoxide form. The latter mineralization of amine substituent and spontaneous oxidation followed by ring opening of phenolic compounds contributed in the formation of CO_2 and H_2O as the final products [20,70].

The total organic carbon ratio (TOC/TOC_0) showed a significant decrease, which may be attributed to the fact that structured dye molecules were fragmented and converted into small organic molecules, thus enhancing mineralization during the irradiation process [71]. In order to provide some evidence, changes in pH were monitored before and after the reaction. This showed that the solution reaction was shifted from pH 11 to pH 7.3, reflecting the fact that the MB dye most probably oxidized and decomposed into CO_2 and H_2O to some extent [72].

3.6. Application to other dyes

In order to study the proficiency and effectiveness of the $EGZrO_2$–EGZnO/HY photocatalyst, various types of dyes such as malachite green (MB), Congo red (CR), and methyl orange (MO) were tested; the results are shown in Fig. 16. The initial concentration of the respective dye was held constant (10 mg L^{-1}) and was prepared using laboratory tap water, then irradiated under fluorescent light for 3 h of contact time. A high decolorization percentage

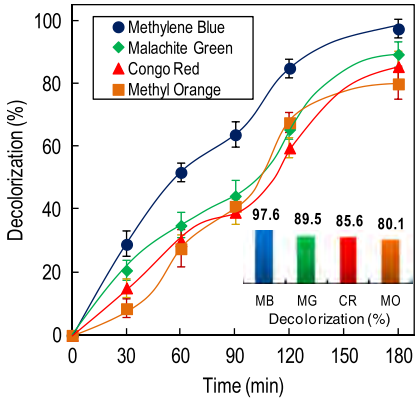

Fig. 16. Application of $EGZrO_2$–EGZnO/HY on photocatalytic decolorization of various types of dye [C_0 = 10 mg L^{-1}, pH = 7, W = 0.60 g L^{-1}, t = 3 h, under fluorescent light].

(>80%) of the various types of dye was obtained, showing the potential of these electrogenerated photocatalysts.

4. Conclusions

In this study, a new one-pot electrosynthesis method of highly photoactive Si coordinated with Zr and Zn catalysts was introduced for efficient degradation of MB. The excellent photoresponse of $EGZrO_2$–EGZnO/HY under visible light conditions was achieved using an amount of 0.60 g L^{-1} of catalyst, resulting in 99.7% MB decolorization after 1.5 h at pH 11 under room temperature. The photocatalytic decolorization of MB followed pseudo first-order kinetics and the rate constants were determined using the Langmuir–Hinshelwood model, and were found to be K_R = 14.3 mg L^{-1} - h^{-1} and K_{LH} = 7.49 L mg^{-1}. This suggested that the dye adsorption was the controlling step of the process. The mineralization of MB was measured by COD removal and TOC/TOC_0 ratio analyses, which were 97.2% and 0.03%, respectively, after 1.5 h of contact time. The catalyst was still stable after five cycling runs and the leaching test showed negligible leaching effects. Malachite green (MG), Congo red (CR), and methyl orange (MO) gives 89.5%, 85.6%, and 80.1% decolorization, respectively, compared to MB (97.6%) using an amount of 0.60 g L^{-1} in 10 mg L^{-1} of initial dye concentration at pH 7 after 3 h of contact time under fluorescent light. Significantly, the simple operation, short synthesis time, high decolorization percentage of MB, and above all, the unique structure of $EGZrO_2$–EGZnO/HY, may make this synthesis method an

obvious choice for the preparation of various catalysts for a variety of applications. However, the exact structure of $EGZrO_2$–EGZnO/HY is still under study.

Acknowledgement

The authors are grateful for the financial support by the Research University Grant from Universiti Teknologi Malaysia (Grant No. 01H59), the awards of UTM Zamalah Scholarship (Norzahir Sapawe) and the Hitachi Scholarship Foundation for their support.

References

[1] V. Sarria, M. Deront, P. Peringer, C. Pulgarin, Degradation of a biorecalcitrant dye precursor present in industrial wastewaters by a new integrated iron (III) photoassisted-biological treatment, Appl. Catal. B: Environ. 40 (2003) 231–246.
[2] M.A.Z. Abidin, A.A. Jalil, S. Triwahyono, S.H. Adam, N.H.N. Kamarudin, Recovery of gold (III) from an aqueous solution onto a durio zibethinus husk, Biochem. Eng. J. 54 (2011) 124–131.
[3] F. Harrelkas, A. Azizi, A. Yaacoubi, A. Benhammou, M.N. Pons, Treatment of textie dye effluents using coagulation–flocculation coupled with membrane processes or adsorption on powdered activated carbon, Desalination 235 (2009) 330–339.
[4] A.A. Jalil, S. Triwahyono, N.A.M. Razali, N.H.H. Hairom, A. Idris, M.N.M. Muhid, A. Ismail, N.A.M. Yahaya, N.A.L. Ahmad, H. Dzinun, Complete electrochemical dechlorination of chlorobenzenes in the presence of various arene mediators, J. Hazard. Mater. 174 (2010) 581–585.
[5] J.S. Wu, L.H. Liu, K.H. Chu, S.Y. Suen, Removal of cationic dye methyl violet 2b from water by cation exchange membranes, J. Membr. Sci. 309 (2008) 239–245.
[6] S. Mozia, M. Tomaszewska, A.W. Morawski, A new photocatalytic membrane reactor (PMR) for removal of azo-dye acid red 18 from water, Appl. Catal. B: Environ. 59 (2005) 131–137.
[7] Z. Zhang, Y. Xu, X. Ma, F. Li, D. Liu, Z. Chen, F. Zhang, D.D. Dionysiou, Microwave degradation of methyl orange dye in aqueous solution in the presence of nano-TiO_2-supported activated carbon (supported-TiO_2/AC/MW), J. Hazard. Mater. 209–210 (2012) 271–277.
[8] N.F. Jaafar, A.A. Jalil, S. Triwahyono, M.N.M. Muhid, N. Sapawe, M.A.H. Satar, H. Asaari, Photodecolorization of methyl orange over α-Fe_2O_3-supported HY catalysts: the effects of catalyst preparation and dealumination, Chem. Eng. J. 191 (2012) 112–122.
[9] M.J. Height, S.E. Pratsinis, O. Mekasuwandumrong, P. Praserthdam, Ag–ZnO catalysts for UV-photodegradation of methylene blue, Appl. Catal. B: Environ. 63 (2006) 305–312.
[10] K. Hayat, M.A. Gondal, M.M. Khaled, S. Ahmed, A.M. Shemsi, Nano ZnO synthesis by modified sol gel method and its application in heterogenous photocatalytic removal of phenol from water, Appl. Catal. A: Gen. 393 (2011) 122–129.
[11] W. Zhou, K. Liu, H. Fu, K. Pan, L. Zhang, L. Wang, C.C. Sun, Multi-modal mesoporous TiO_2–ZrO_2 composite with high photocatalytic activity and hydrophilicity, Nanotechnology 19 (2008) 1–7.
[12] J.Y. Kim, J.W. Jang, D.H. Youn, J.Y. Kim, E.S. Kim, J.S. Lee, Graphene–carbon nanotube composite as an effective conducting scaffold to enhance the photoelectrochemical water oxidation activity of a hematite film, RSC Adv. 2 (2012) 9415–9422.
[13] F. Meng, J. Li, S.K. Cushing, J. Bright, M. Zhi, J.D. Rowley, Z. Hong, A. Manivannan, A.D. Bristow, N. Wu, Photocatalytic water oxidation by hematite/reduced graphene oxide composites, ACS Catal. 3 (2013) 746–751.
[14] H. Ma, L. Yue, C. Yu, X. Dong, X. Zhang, M. Xue, X. Zhang, Y. Fu, Synthesis, characterization and photocatalytic activity of Cu-doped Zn/ZnO photocatalyst with carbon modification, J. Mater. Chem. 22 (2012) 23780–23788.
[15] X. Yang, C. Cao, L. Erickson, K. Hohn, R. Maghirang, L. Klabunde, Photo-catalytic degradation of Rhodamine B on C-, S-, N-, and Fe-doped TiO_2 under visible-light irradiation, Appl. Catal. B: Environ. 91 (2009) 657–662.
[16] J.H. Sun, S.Y. Dong, J.L. Feng, X.J. Yin, X.C. Zhao, Enhanced sunlight photocatalytic performance of Sn-doped ZnO for methylene blue degradation, J. Mol. Catal. A: Chem. 335 (2011) 145–150.
[17] W. Zhao, L. Feng, R. Yang, J. Zheng, X. Li, Characterization, and photocatalytic properties of Ag modified hollow SiO_2/TiO_2 hybrid microspheres, Appl. Catal. B: Environ. 103 (2011) 181–189.
[18] W. Zhang, K. Wang, Y. Yu, H. He, TiO_2/HZSM-5 nano-composite photocatalyst: HCl treatment of NAZSM-5 promotes photocatalytic degradation of methyl orange, Chem. Eng. J. 163 (2010) 62–67.
[19] Z.M. El-Bahy, M.M. Mohamed, F.I. Zidan, M.S. Thabet, Photo-degradation of acid green dye over Co–ZSM-5 catalysts prepared by incipient wetness impregnation technique, J. Hazard. Mater. 153 (2008) 364–371.
[20] A. Nezamzadeh-Ejhieh, S. Hushmandrad, Solar photodecolorization of methylene blue by CuO/X zeolite as a heterogeneous catalyst, Appl. Catal. A: Gen. 388 (2010) 149–159.
[21] A. Nezamzadeh-Ejhieh, Z. Salimi, Solar photocatalytic degradation of o-phenylenediamine by heterogeneous CuO/X zeolite catalyst, Desalination 280 (2011) 281–287.
[22] A. Nezamzadeh–Ejhieh, Z. Salimi, Heterogeneous photodegradation catalysis of o-phenylenediamine using CuO/X zeolite, Appl. Catal. A: Gen. 390 (2010) 110–118.
[23] A. Nezamzadeh–Ejhieh, Z. Banan, A comparison between the efficiency of CdS nanoparticles/zeolite A and CdO/zeolite A as catalysts in photodecolorization of crystal violet, Desalination 279 (2011) 146–151.
[24] H. Chen, A. Matsumoto, N. Nishimiya, K. Tsutsumi, Preparation and characterization of TiO_2 incorporated Y-zeolite, Colloids Surf. 57 (1999) 295–305.
[25] M. Alvaro, E. Carbonell, M. Espla, H. Garcia, Iron phthalocyanine supported on silica or encapsulated inside zeolite Y as solid photocatalysts for the degradation of phenols and sulfur heterocycles, Appl. Catal. B: Environ. 57 (2005) 37–42.
[26] M. Aleksic, H. Kusic, N. Koprivanac, D. Leszczynska, A.L. Bozic, Heterogeneous fenton type processes for the degradation of organic dye pollutant in water: the application of zeolite assissted AOPs, Desalination 257 (2010) 22–29.
[27] S. Triwahyono, A.A. Jalil, M. Musthofa, S. Triwahyono, A.A. Jalil, M. Musthofa, Generation of protonic acid sites from pentane on the surfaces of Pt/SO_4^{2-}–ZrO_2 and Zn/H–ZSM5 evidenced by IR study of adsorbed pyridine, Appl. Catal. A: Gen. 372 (2010) 90–93.
[28] N. Sapawe, A.A. Jalil, S. Triwahyono, S.H. Adam, N.F. Jaafar, M.A.H. Satar, Isomorphous substitution of Zr in the framework of aluminosilicate HY by an electrochemical method: evaluation by methylene blue decolorization, Appl. Catal. B: Environ. 125 (2012) 311–323.
[29] N. Sapawe, A.A. Jalil, S. Triwahyono, R.N.R.A. Sah, N.W.C. Jusoh, N.H.H. Hairom, J. Efendi, Electrochemical strategy for grown ZnO nanoparticles deposited onto HY zeolite with enhanced photodecolorization of methylene blue: Effect of the formation of Si–O–Zn bonds, Appl. Catal. A: Gen. 456 (2013) 144–158.
[30] N. Chandra, D.K. Singh, M. Sharma, R.K. Upadhyay, S.S. Amritphale, S.K. Sanghi, Synthesis and characterization of nanosized zirconia powder synthesized by single emulsion-assisted direct precipitation, J. Colloid Interf. Sci. 342 (2010) 327–332.
[31] L.Y. Zhu, X.Q. Wang, G.H. Zhang, Q. Ren, D. Xu, Structural characterization and photocatalytic activity of B_2O_3/ZrO_2–TiO_2 mesoporous fibers, Appl. Catal. B: Environ. 103 (2011) 428–435.
[32] Y. Chen, S.K. Lunsford, Y. Song, H. Ju, P. Falaras, V. Likodimos, A.G. Kontos, D.D. Dionysiou, Synthesis, characterization and electrochemical properties of mesoporous zirconia nanomaterials prepared by self-assembling sol–gel method with Tween 20 as a template, Chem. Eng. J. 170 (2011) 518–524.
[33] A.A. Jalil, N. Kurono, M. Tokuda, Facile synthesis of ethyl-2-arylpropenoates by cross-coupling reaction using EG-highly reactive zinc, Tetrahedron 58 (2002) 7477–7484.
[34] A.A. Jalil, N. Kurono, M. Tokuda, Facile synthesis of 2-arylpropenoic acid esters by cross-coupling using electrogenerated highly reactive zinc and a palladium catalyst, Synlett 12 (2001) 1944–1946.
[35] B. Wu, R. Yuan, X. Fu, Structural characterization and photocatalytic activity of hollow binary ZrO_2/TiO_2 oxide fibers, J. Solid State Chem. 182 (2009) 560–565.
[36] R. Anand, S.G. Hegde, B.S. Rao, C.S. Gopinath, Catalytic synthesis of 2-methyl pyrazine over Zn-modified zeolites, Catal. Lett. 84 (2002) 265–272.
[37] A. Susarrey-Arce, M.A. Hernandez-Espinosa, F. Rojas-Gonzalez, C. Reed, V. Petranovskii, A. Licea, Inception and trapping of ZnO nanoparticles within desilicated mordenite and ZSM-5 zeolites, Part. Part. Syst. Charact. 27 (2010) 100–111.
[38] D.T. Harvey, R.W. Linton, X-ray photoelectron spectroscopy (XPS) of adsorbed zinc on amorphous hydrous ferric oxide, Colloids Surf. 11 (1984) 81–96.
[39] D. Barreca, M.P. Copley, A.E. Graham, J.D. Holmes, M.A. Morris, R. Seraglia, T.R. Spalding, E. Tondello, Methanolysis of styrene oxide catalysed by a highly efficient zirconium-doped mesoporous silica, Appl. Catal. A: Gen. 304 (2006) 14–20.
[40] J.V. Kingston, J.G. Verkade, P[N(^{t}Bu)CH_2CH_2]$_3$N: a versatile non-ionic base for the synthesis of higher coordinate silicates, Inorg. Chem. Commun. 8 (2005) 643–646.
[41] S. Prabakar, K.J. Rao, C.N.R. Rao, A MAS NMR investigation of lead phosphosilicate glasses: the nature of the highly deshielded six-coordinated silicon, Mater. Res. Bull. 26 (1991) 285–294.
[42] R. Tacke, M. Penka, F. Popp, R. Ingo, Bis[citrate(3-)-O1, O3, O6] silicate: A dianionic complex with hexacoordinate silicon (IV) and two tridentate dioato (2-) olato (1-) ligands, Eur. J. Inorg. Chem. 5 (2002) 1025–1028.
[43] J. Klinowski, Solid-state NMR studies of molecular sieve catalysts, Chem. Rev. 91 (1991) 1459–1479.
[44] K.S. Smirnov, Computer modeling study of interaction of acetonitrile hydroxyl groups of HY, J. Phys. Chem. B 105 (2001) 7405–7413.
[45] C. Wang, H. Shi, Y. Li, Synthesis and characteristics of natural zeolite supported Fe^{3+}–TiO_2 photocatalysts, Appl. Surf. Sci. 257 (2011) 6873–6877.
[46] S. Kongwudthiti, P. Praserthdam, W. Tanakulrungsank, M. Inoue, The influence of Si–O–Zr bonds on the crystal-growth inhibition of zirconia prepared by the glycothermal method, J. Mater. Process. Technol. 136 (2003) 186–189.
[47] J.W. Soares, J.E. Whitten, D.W. Oblas, D.M. Steeves, Novel photoluminescence properties of surface-modified nanocrystalline zinc oxide: toward a reactive scaffold, Langmuir 24 (2008) 371–374.
[48] Q. Chang, J.E. Zhou, Y. Wang, G. Meng, Preparation and characterization of unique zirconia crystal within pores via sol–gel-hydrothermal method, Adv. Powder Technol. 20 (2009) 371–374.

[49] Y. Chen, S. Lunsford, D.D. Dionysiou, Characterization and electrochemical response of sonogel carbon electrode modified with nanostructured zirconium dioxide film, Sens. Actuat. B: Chem. 137 (2009) 291–296.
[50] D.P. Das, N. Baliarsingh, K.M. Parida, Photocatalytic decolorization of methylene blue (MB) over titania pillared zirconium phosphate (ZrP) and titanium phosphate (TiP) under solar radiation, J. Mol. Catal. A: Chem. 261 (2007) 254–261.
[51] R. Chatti, S.S. Rayalu, N. Dubey, N. Labhsetwar, S. Devotta, Solar-based photoreduction of methyl orange using zeolite supported photocatalytic materials, Solar Energy Mater. Solar Cells 91 (2007) 180–190.
[52] M. Pelaez, N.T. Nolan, S.C. Pillai, M.K. Seery, P. Falaras, A.G. Kontos, P.S.M. Dunlop, J.W.J. Hamilton, J.A. Byrne, K. O'Shea, M.H. Entezari, D.D. Dionysiou, A review on the visible light active titanium dioxide photocatalysts for environmental applications, Appl. Catal. B: Environ. 125 (2012) 331–349.
[53] C. Han, M. Pelaez, V. Likodimos, A.G. Kontos, P. Falaras, K. O'Shea, D.D. Dionysiou, Innovative visible light-activated sulfur doped TiO_2 films for water treatment, Appl. Catal. B: Environ. 107 (2011) 77–87.
[54] H. Jia, H. Xu, Y. Hu, Y. Tang, L. Zhang, TiO_2@CdS core–shell nanorods films: fabrication and dramatically enhanced photoelectrochemical properties, Electrochem. Commun. 9 (2007) 354–360.
[55] J. Portier, H.S. Hilal, I. Saadeddin, S.J. Hwang, M.A. Subramanian, G. Campet, Thermodynamic correlations and band gap calculations in metal oxides, Prog. Solid State Chem. 32 (2004) 207–217.
[56] G.H. Kuhl, Coordination of aluminum and silicon in zeolites as studied by X-ray spectrometry, J. Phys. Chem. Solids 38 (1977) 1259–1263.
[57] R.J.P. Corriu, G. Dabosi, M. Martineau, Mécanisme de l'hydrolyse des chlorosilanes, catalysée par un nucléophile: étude cinétique et mise en evidence d'un intermediaire hexacoordonné, J. Organomet. Chem. 150 (1978) 27–38.
[58] S. Krijnen, Titanium epoxidation catalyts: zeolite and silsesquioxane based materials, Eindhoven University of Technology, Netherlands, 1998.
[59] M.A. Behnajady, N. Modirshala, R. Hamzavi, Kinetic study on photocatalytic degradation of C.I. acid yellow 23 by ZnO photocatalyst, J. Hazard. Mater. B133 (2006) 226–232.
[60] A. Franco, M.C. Neves, M.M.L. Mobteiro, Photocatalytic decolorization of methylene blue in the presence of TiO_2/ZnS nanocomposites, J. Hazard. Mater. 161 (2009) 545–550.
[61] S.K. Kansal, A.H. Ali, S. Kapoor, Photocatalytic decolorization of biebrich scarlet dye in aqueous phase using different nanophotocatalysts, Desalination 259 (2010) 147–155.
[62] B. Beverskog, I. Puigdomenech, Revised pourbaix diagrams for zinc at 25–300°C, Corros. Sci. 39 (1997) 107–114.
[63] E. Bizani, K. Fytianos, I. Poulios, V. Tsiridis, Photocatalytic decolorization and degradation of dye solutions and wastewaters in the presence of titanium dioxide, J. Hazard. Mater. 1367 (2006) 85–94.
[64] H. Lachheb, E. Puzenat, A. Houas, M. Ksibi, E. Elaloui, C. Guillard, J.M. Herrmann, Photocataytic degradation of various types of dyes (Alizarin S, Crocein Orange G, Methyl Red, Congo Red, methylene blue in water by UV-irradiated titinia, Appl. Catal. B: Environ. 39 (2002) 75–90.
[65] C.S. Turchi, D.F. Ollis, Photocatalytic degradation of organic water contaminants: mechanisms involving hydroxyl radical attack, J. Catal. 122 (1990) 178–192.
[66] J. Grzechulska, A.W. Morawski, Photocatalytic decomposition of azo-dye acid black 1 in water over modified titanium dioxide, Appl. Catal. B: Environ. 36 (2002) 45–51.
[67] L.Y. Yang, S.Y. Dong, J.H. Sun, J.L. Feng, Q.H. Wu, S.P. Sun, Microwave-assisted preparation, characterization and photocatalytic properties of a dumbbell-shaped ZnO photocatalyst, J. Hazard. Mater. 179 (2010) 438–443.
[68] R.A. Palominos, A. Mora, M.A. Mondaca, M. Perez–Moya, H.D. Mansilla, Oxolinic acid photo-oxidation using immobilized TiO_2, J. Hazard. Mater. 158 (2008) 460–464.
[69] J. Sun, X. Wang, J. Sun, R. Sun, L. Qiao, Photocatalytic degradation and kinetic of orange G using nano-sizes Sn(IV)/TiO_2/AC photocatalyst, J. Mol. Catal. A: Chem. 260 (2006) 241–246.
[70] A. Houas, H. Lachheb, M. Ksibi, E. Elaloui, C. Guillard, J.M. Herrmann, Photocatalytic degradation pathway of methylene blue in water, Appl. Catal. B: Environ. 31 (2001) 145–157.
[71] J. Paul, K.P. Rawat, K.S.S. Sarma, S. Sabharwal, Decoloration and degradation of reactive red-120 dye by electron beam irradiation in aqueous solution, Appl. Radiat. Isot. 69 (2011) 982–987.
[72] X. Li, K. Lv, K. Deng, J. Tang, R. Su, J. Sun, L. Chen, Synthesis and characterization of ZnO and TiO_2 hollow spheres with enhanced photoreactivity, Mater. Sci. Eng. B 158 (2009) 40–47.